Science of the Total Environment 627 (2018) 235–244

Contents lists available at ScienceDirect

Science of the Total Environment

journal homepage: www.elsevier.com/locate/scitotenv

Adsorption of tetracycline antibiotics from aqueous solutions on nanocomposite multi-walled carbon nanotube functionalized MIL-53 (Fe) as new adsorbent

Weiping Xiong [a,b], Guangming Zeng [a,b,*], Zhaohui Yang [a,b,*], Yaoyu Zhou [c], Chen Zhang [a,b], Min Cheng [a,b], Yang Liu [a,b], Liang Hu [a,b], Jia Wan [a,b], Chengyun Zhou [a,b], Rui Xu [a,b], Xin Li [a,b]

[a] College of Environmental Science and Engineering, Hunan University, Changsha 410082, China
[b] Key Laboratory of Environmental Biology and Pollution Control, Ministry of Education, Hunan University, Changsha 410082, China
[c] College of Resources and Environment, Hunan Agricultural University, Changsha 410128, China

HIGHLIGHTS

- Multi-walled carbon nanotube modified MIL-53(Fe) was used to remove antibiotic tetracycline for the first time.
- MWCNT/MIL-53(Fe) showed the highest adsorption capacity for TCN, OTC and CTC, respectively.
- π-π interactions were possible mechanism for adsorptive removal of TCN, OTC and CTC.
- MWCNT/MIL-53(Fe) with great water stability was suggested as a reusable and efficient adsorbent.

GRAPHICAL ABSTRACT

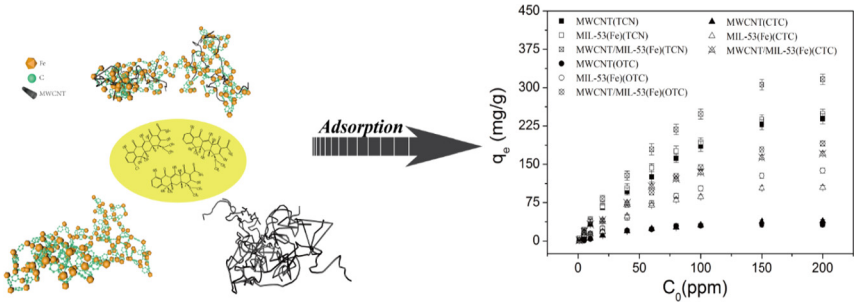

ARTICLE INFO

Article history:
Received 1 December 2017
Received in revised form 17 January 2018
Accepted 24 January 2018
Available online xxxx

Editor: Baoliang Chen

Keywords:
Adsorption
Tetracycline antibiotics
π-π interactions
MWCNT nanocomposite

ABSTRACT

Adsorption of tetracycline antibiotics from aqueous solutions by a multi-walled carbon nanotube (MWCNT) loaded iron metal-organic framework (MIL-53(Fe)) composite was studied. The adsorbent was characterized by environmental scanning electron microscope, energy dispersive X-ray spectroscopy, brunauer-emmett-teller, thermogravimetric analysis, X-ray diffraction, fourier transform infrared spectrum, and X-ray photoelectron spectrum. The adsorption kinetics of tetracycline hydrochloride (TCN), oxytetracycline hydrochloride (OTC), and chlortetracycline hydrochloride (CTC) were all well fitted to the pseudo-second-order equation as well as the adsorption isotherms could be well delineated via Langmuir equations. The main influencing factors such as pH and ionic strength were studied in detail. At initial pH of 7.0, maximum adsorption capacity of TCN, OTC and CTC on MWCNT/MIL-53(Fe) was 364.37, 325.59, 180.68 mg·g^{-1} at 25 °C, which was 1.25, 8.28 and 3.34 times than that of single MWCNT, respectively. The adsorption capacity of TCS for this adsorbent was in the order: TCN > OTC > CTC, which was determined by the adsorbate molecule magnitude. In addition, π-π adsorbate-adsorbent interactions played an important role during the adsorption process. The excellent reusability and great water stability indicated the potential application of this novel composite in the removal of TCS from aqueous solutions.

1. Introduction

Pharmaceuticals and personal care products (PPCPs) as representative emerging contaminants (Seo et al., 2017; Z.M. Liu et al., 2017; X.C.

* Corresponding authors at: Hunan University, College of Environmental Science and Engineering, Changsha 410082, China.
E-mail addresses: zgming@hnu.edu.cn (G. Zeng), yzh@hnu.edu.cn (Z. Yang).

https://doi.org/10.1016/j.scitotenv.2018.01.249
0048-9697/

Liu et al., 2017a, 2017b; Chen et al., 2015) have received wide attention due to their persistent existence in surface/ground water (Evgenidou et al., 2015; Hasan et al., 2016; Tang et al., 2014). Even more serious situation is that several PPCPs have already found in the tissues of fishes and vegetables (Ramirez et al., 2009; Wu et al., 2014; Tanoue et al., 2015). If PPCPs are ingested by a variety of ways, they probably cause endocrine disruptions and result in profound influence on human health. Antibiotic, especially tetracycline antibiotics (TCS) is one of the typical PPCPs (Qiang and Adams, 2004; Azhar et al., 2016). TCS, mainly including tetracycline hydrochloride (TCN) (H. Wang et al., 2016; C.H. Wang et al., 2016), oxytetracycline hydrochloride (OTC) (Hu et al., 2016) and chlortetracycline hydrochloride (CTC) (Ye et al., 2017) has been widely used for prevention of infectious in animals and humans for a long time. The increasing use of TCS in many fields brings a lot of environmental issues. However, removal of TCS from aqueous solutions is difficult due to its changeful occurrence state, low biodegradability, and complexity of molecular structures (Seo et al., 2017). Therefore, the high-efficiency removal of TCS from aquatic system has already become a major concern.

Various methods, such as biodegradation (H.F. Xiong et al., 2017; W.P. Xiong et al., 2017; Hu et al., 2017), biofiltration (Y. Cheng et al., 2016; M. Cheng, et al., 2016a, 2016b; Yang et al., 2010), advanced oxidation processes (AOPs) (Y. Cheng et al., 2016; M. Cheng, et al., 2016a, 2016b), electrochemistry (Zhang et al., 2015; Zhang et al., 2016a, 2016b), photocatalytic degradation (Tanoue et al., 2015; Hu et al., 2016; Xu et al., 2012a, 2012b; Zhou et al., 2018), membrane filtration (Z.M. Liu et al., 2017; X.C. Liu et al., 2017a, 2017b) and adsorption (Gong et al., 2009; Deng et al., 2013; Xu et al., 2012a, 2012b; Tan et al., 2015; Long et al., 2011; Zeng et al., 2017) have been tested for the removal of PPCPs. However, adsorption has been advised as a very competitive method to get rid of PPCPs from aqueous solutions in consideration of its low cost, simple operation and no secondary pollution. Nevertheless, an appropriate adsorbent is urgently needed (Zhou et al., 2017a; Liang et al., 2017; Z.B. Wu et al., 2016; H.P. Wu et al., 2016). Recently, as a porous functional material, metal-organic frameworks (MOFs) which are consisted of various organic linkers and metal ions (or clusters) (Furukawa et al., 2013; Azhar et al., 2017), attract much attention on adsorption, besides, including catalysis, sensing and gas storage owing to their ultrahigh porosity, large surface area, tunable pore size/shape, and easy functionalization (Barea et al., 2014; Hwang et al., 2008). MOFs have been used in removal of harmful substances from both gaseous and liquid phase (Khan et al., 2013; Reed et al., 2016; Voorde et al., 2014). Nevertheless, previous work indicated that the use of MOFs as adsorbents in gaseous phase was more than in liquid phase due to the lability of MOFs in aqueous solutions (Z.M. Liu et al., 2017; X.C. Liu et al., 2017a, 2017b).

Fortunately, a higher confidence about the water stability of MOFs was reported in the literature recently (Azhar et al., 2018). For examples, researchers (Cadiaul et al., 2017) reported hydrolytically stable fluorinated MOFs, $NiAlF_5(H_2O)(pyr)_2{\cdot}2(H_2O)$(KAUST-8, AlFFIVE-1-Ni) and $NiFeF_5(H_2O)(pyr)_2{\cdot}4(H_2O)$(KAUST-9, FeFFIVE-1-Ni), to remove water from gas streams. Some researchers (Yang et al., 2009; Rehman et al., 2017) synthesized two kind of MWCNT@MOF-5 hybrid composites to improve hydrophobic properties, respectively. Researchers (Wu et al., 2010) reported a modular construction of a new MOF by incorporating plenty of water repellent functional groups in the frameworks to enhance its stability in humid air. Nevertheless, the removal of TCS by adsorption has merely been presented with these adsorbents such as graphene oxide (Yu et al., 2017), nano zero valent iron (Guo et al., 2017), activated carbons (Ahmed, 2017) and activated carbon fiber (Thi and Lee, 2017), while the MWCNT loaded MOFs as a kind of adsorbent for the removal of TCS from aqueous solutions have rarely been reported. MIL-53(M) family is different from other MOFs, their chemical versatility of flexible structure and breathing feature and stability has taken up a prominent circumstance (Naeimi and Faghihian, 2017). Besides, the high-valence Fe^{3+} metal ion with common carboxylate-type ligands could synthesize a water stable MOF (Z.M. Liu et al., 2017; X.C. Liu et al., 2017a, 2017b; H. Wang et al., 2016; C.H. Wang et al., 2016).

Hence, we synthesized a kind of MWCNT/MIL-53(Fe) composite to remove TCS, i.e., TCN, OTC and CTC from aqueous solutions, simultaneously. The adsorption kinetics, adsorption isotherms and adsorption mechanisms were studied in detail. Furthermore, the experiment influencing factors, i.e., reaction time, pH, ionic strength and reusability were analyzed synthetically. Finally, the water stability of MWCNT/MIL-53(Fe) was also investigated. These superior properties of MWCNT/MIL-53(Fe) indicated that it could be applied to treatment of antibiotic wastewater.

2. Experimental

2.1. Materials and reagents

N,N-dimethylformamide (DMF) (99.5%), ferric chloride hexahydrate ($FeCl_3{\cdot}6H_2O$) (99%), 1,4-benzenedicarboxylic acid (1,4-BDC) (99%) and ethanol (99.5%) were purchased from Sinopharm Chemical Regent Co., Ltd. (Shanghai, China). Multi-walled carbon nanotube (MWCNT) with diameters ranging from 10 to 20 nm was purchased from the Chengdu Organic Chemicals Co. Ltd. TCN, OTC and CTC were obtained from Bomei biotechnology Co., Ltd. (Hefei, China). All other reagents and solvents were analytical grade and used as received without any other purification. The ultra-pure water (resistivity of 18.25 $M\Omega{\cdot}cm^{-1}$) was used throughout the experiment.

2.2. Synthesis of adsorbents

2.2.1. Synthesis of MIL-53(Fe)

MIL-53(Fe) was prepared by solvothermal method (Yang et al., 2016). In a typical procedure, 0.674 g of $FeCl_3{\cdot}6H_2O$ and 0.415 g of 1, 4-BDC were added into 56 mL of DMF solution. The mixture was stirred at room temperature for 1 h, and then transferred into a 100 mL Teflon-lined stainless steel autoclave. After that, the autoclave was heated at 170 °C for 24 h. The products were collected by centrifugation at 5000 rpm, washed with DMF and ethanol, repeatedly. The yellow powder was finally filtered and dried in vacuum at 100 °C for 10 h.

2.2.2. Synthesis of MWCNT/MIL-53(Fe)

MWCNT (PR China) was soaked in mixed acid (a mixture of nitric acid and sulfuric acid) at 80 °C under stirring for 24 h, functionalizing carboxylic groups at the defect sites (Eguilaz et al., 2011). After it was filtered, washed with deionized water, and dried at 70 °C, the obtained powder denoted as purified MWCNT.

For synthesis of MWCNT/MIL-53(Fe) in variable proportions, different amounts of purified MWCNT (1, 5, 10, 20 and 30 wt%) were dispersed in DMF and then this mixture was mixed with solution of ferric chloride hexahydrate (0.674 g), 1,4-Benzenedicarboxylic acid (0.415 g) and DMF. The resulting mixture was stirred for some time at room temperature, then transferred into a 100 mL Teflon liner in stainless steel autoclave and heated at 170 °C for 24 h. The powder was collected, washed with DMF and ethanol, and dried under vacuum at 100 °C for 10 h.

2.3. Characterization methods

The morphologies of MWCNT, MIL-53(Fe) and MWCNT/MIL-53(Fe) were observed via environmental scanning electron microscope (SEM) (Carl Zeiss, EVO-MA10, Germany). Energy dispersive X-ray spectroscopy (EDS) of the materials was obtained using an energy dispersive X-ray detector (Oxford Instruments, UK). The Brunauer-Emmett-Teller (BET) specific surface area and pore volume and pore size of materials were measured by automatic surface analyzer (Quantachrome, USA). The crystal phase of materials was obtained by a D8 X-ray diffractometer (XRD; Bruker, Germany). Binding energies were determined by X-

ray photoelectron spectrum (XPS) (Thermo Fisher Scientific-ESCALAB 250Xi, USA). Thermogravimetric analysis (TGA) was measured by a Mettler TGA/SDT Q600 analyzer. The Fourier transform infrared spectrum (FT-IR) measurements were obtained from a Nicolet 5700 Spectrometer in KBr pellet at room temperature (Nicolet, USA). The zeta potential of MWCNT/MIL-53(Fe) was measured by a Zeta potential analyzer (Zetasizer Nano zs90) at varying pH values.

2.4. Adsorption experiments

The adsorbents of MWCNT, MIL-53(Fe) and MWCNT/MIL-53(Fe) (in variable proportions) were dried for 8 h in a vacuum oven and used for adsorption of the TCS in aqueous solutions. The TCS solutions of the batch experiments were prepared for each TCS stock solution (200 $mg \cdot L^{-1}$) in deionized water. Different concentrations of solutions (1–200 $mg \cdot L^{-1}$) were obtained by using deionized water to dilute the stock solution. The adsorption kinetics for TCS over adsorbents were obtained by adsorption with each TCS concentration of 20 $mg \cdot L^{-1}$ in solution. At predetermined time intervals, 1 mL of solution was taken out. The adsorption isotherms were run with duplicate points of TCS to adsorbents, for which adsorbents adding to solution with TCS concentration between 1 $mg \cdot L^{-1}$ and 200 $mg \cdot L^{-1}$. The effect of pH on the amount of TCS adsorbed by the adsorbents was tested with pH values from 3 to 9. The pH value of the TCS solutions (20 $mg \cdot L^{-1}$) was adjusted by using a pH meter (FE20, China) with aqueous NaOH (0.1 M) or HCl (0.1 M). The impact of ionic strength on adsorption was determined using 20 $mg \cdot L^{-1}$ TCS solution containing 1–9 $g \cdot L^{-1}$ of NaCl and adsorbents. The water stability of MIL-53(Fe) and MWCNT/MIL-53(Fe) was mainly determined by the iron ion concentration in solution.

After spiking with TCS and other solutes, the mixture was equilibrated at 200 rpm (25 °C) on a gyratory shaker. The samples were centrifuged at 5000 rpm for 10 min (25 °C), and then the solution was filtered using 0.45 μm PVDF disposable filters prior to UV spectrophotometer (UV-2700, SHIMADZU, Japan). The concentration of iron ion in the solution was measured by a DR2000 spectrophotometer (Hach, USA) using the 1, 10-phenanthroline-based method. All of the experiments were performed in triplicates.

3. Results and discussion

3.1. Characterization of the prepared adsorbents

The prepared adsorbents were characterized with different analysis methods. The SEM images and EDS analysis of prepared adsorbents were presented in Fig. 1. It was observed that the MIL-53(Fe) was crystallized in rod like structures (Fig. 1a), which was fairly similar to the previous literature (Araya et al., 2017). The introductions of MWCNT (Fig. 1b) brought an obvious change in the surface morphology of MIL-53(Fe). Furthermore, it was observed that the SEM images of MWCNT/MIL-53(Fe) (Fig. 1c) showed an intimate contact between the original MOFs and MWCNT. The MWCNT was attached on the surface and in the original MOFs structures. EDS analysis of the MWCNT/MIL-53(Fe) showed that it mainly consisted of Fe, C and O (Fig. 1d).

The BET specific surface area and textural properties of composites were thoroughly determined by N_2 adsorption-desorption analysis and the non-local density functional theory (NLDFT) method, and the results were presented in Fig. 2 and Table 1. It could be seen that all curves were type IV isotherms typically with a type H_3 hysteresis, due to the presence of mesoporous and macroporous (Song et al., 2015). It should be noted that the N_2 adsorption-desorption isotherm for MWCNT/MIL-53(Fe) was above that of MIL-53(Fe), indicating that the specific surface area of the samples was increased after MWCNT composited with MIL-53(Fe). The MWCNT/MIL-53(Fe) exhibited the largest volume of mesoporous and macroporous, which was consistent with the result of BET specific surface area measurement in Table 1. As seen in Fig. 2b, the pore size distribution of the composites calculated via the non-local density functional theory (NLDFT) method also confirmed the pore size viewpoint.

The TGA profiles of MWCNT/MIL-53(Fe) exhibited a slightly higher thermal stability due to the introduction of MWCNT (Fig. 3). MIL-53 (Fe) showed the initial weight loss below 340 °C (15.29%), which was

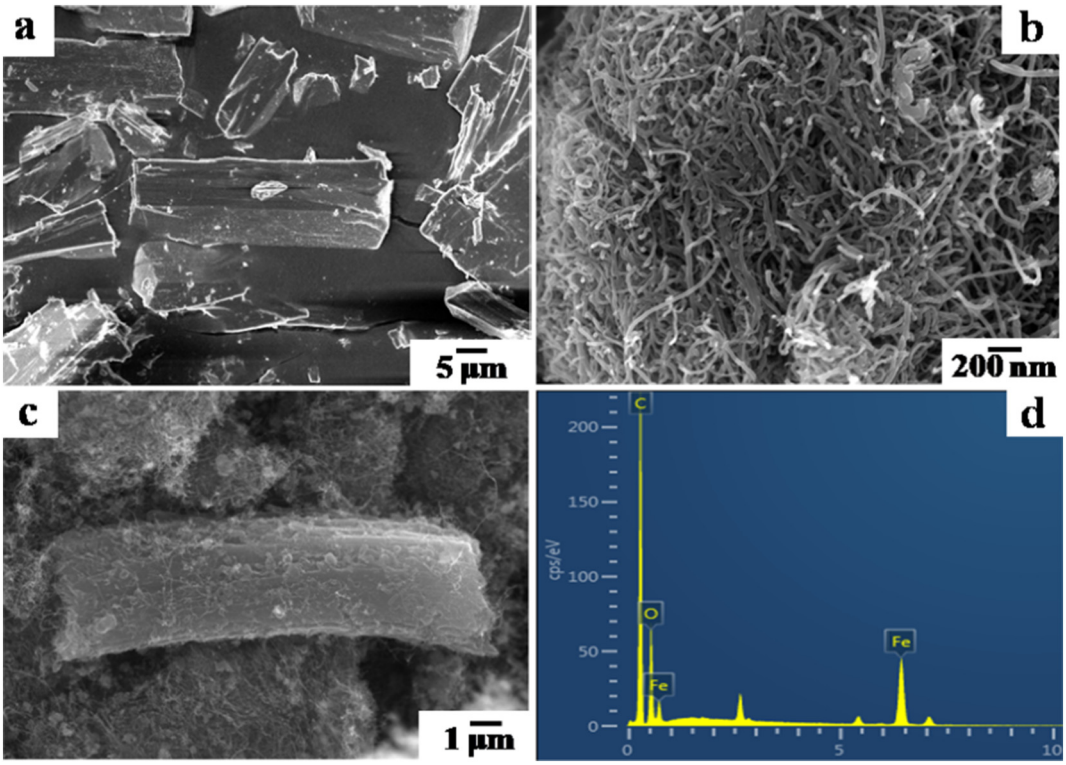

Fig. 1. The SEM images of MIL-53(Fe) (a), MWCNT (b) and MWCNT/MIL-53(Fe)-20% (c); EDS patterns of MWCNT/MIL-53(Fe)-20% (d).

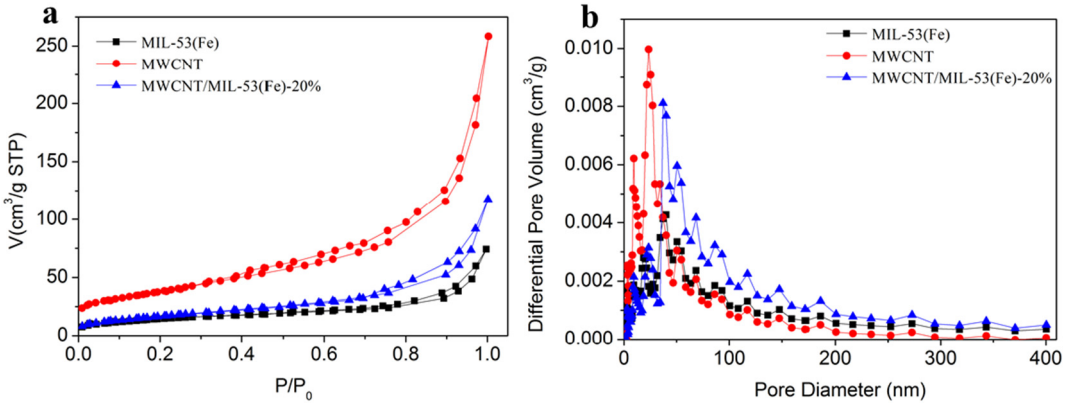

Fig. 2. N_2 adsorption-desorption isotherms (a) and pore size distribution (b) of MIL-53(Fe), MWCNT and MWCNT/MIL-53(Fe)-20%.

attributed to the loss of solvents from the framework. The second weight loss (in the range from 340 to 425 °C (51.26%)) showed the collapse of MIL-53(Fe) structure due to the removal of structural organic ligands from their frameworks. When the temperature attained 425–800 °C, little change in the TG curve was observed. Furthermore, MWCNT in MIL-53(Fe) enhanced their thermal stability, as certified by a rise in decomposition temperature from 340 to 800 °C. The reason was that MIL-53(Fe) crystals were formed by heterogeneous nucleation and crystals growth on MWCNT carboxylate groups acted as nucleation sites (Yang et al., 2009).

As seen in Fig. 4a, the X-ray diffraction (XRD) pattern for virgin MIL-53(Fe) was in perfect agreement with the earlier reported MIL-53(Fe) structure, confirming the successful synthesis of MIL-53(Fe) (Ai et al., 2013). The XRD patterns of the x-MWCNT/MIL-53(Fe) (x = 1, 5, 10, 20 and 30 wt%) composites showed the characteristic diffraction peaks of both MWCNT and MIL-53(Fe), attesting the presence of MWCNT and MIL-53(Fe). Obviously, the diffraction peaks of MWCNT in the composites were reinforced with the increasing in mass ratios of MWCNT to MIL-53(Fe). Although the characteristic peaks of MIL-53 (Fe) became weaker with the increased of MWCNT in the composites, the structure of MIL-53(Fe) wasn't disturbed or destroyed by MWCNT.

In order to in-depth analysis of the molecular structure and ascertain the functional groups of samples, the FT-IR spectroscopy was performed and the results were presented in Fig. 4b. Characteristic peaks of Fe—O (538 cm^{-1}), C—H (750 cm^{-1}), C—O (1390 and 1540 cm^{-1}) and C═O (1650 cm^{-1}) were observed for MIL-53(Fe) (Gao et al., 2017). After MWCNT incorporation, two peaks of O—H (2360 cm^{-1}) and O—H (stretch from H-bonded-COOH, 3450 cm^{-1}) were observed for MWCNT/MIL-53(Fe). Therefore, the results of FT-IR spectra obviously verified the formation of MIL-53(Fe) and MWCNT/MIL-53(Fe) structures, as well as the results of XRD analysis.

The surface chemical state of MWCNT/MIL-53(Fe) was analyzed by X-ray photoelectron spectroscopy (XPS). As presented in Fig. 5, the XPS survey spectrum verified the presence of C, O, Fe in the MWCNT/MIL-53(Fe), which was consistent with analysis of EDS in Fig. 1. The high-resolution XPS spectrum in Fig. 5c of C 1s was fitted into four peaks with the binding energies at 284.65 eV, 284.83 eV, 286.21 eV and 289.36 eV, corresponding to the C═C, C—C, C—O and C═O, respectively. The peak at 284.65 eV of C═C mainly resulted from the benzene rings (Yang et al., 2016). The peaks at 284.83 eV and 286.21 eV corresponded to C—C, C—O in MWCNT (Zhang et al., 2016a, 2016b). The C═O of organic linkers in MWCNT/MIL-53(Fe) and carboxylate groups in MWCNT was at the binding energy of 289.36 eV (Huang et al., 2014). For the XPS spectrum of Fe 2p (Fig. 5b), the peak at 725.83 eV was ascribed to Fe $2p_{1/2}$ and the peak at 712.87 eV was assigned to Fe $2p_{3/2}$, which were representatives of ferric iron in MIL-53(Fe) (Du et al., 2011). Fig. 5d showed that the high resolution XPS of O 1s was suitable for two peaks at 531.86 and 532.38 eV, which could be separately attributed to the oxygen atoms on the H_2BDC linkers and the Fe—O bonds of MIL-53(Fe) (Liang et al., 2015). Hence, the successful composition of samples was proved once again.

3.2. Adsorption of TCS by the adsorbents

Different mass ratios of MWCNT to MIL-53(Fe) in the composites showed different adsorption ability to TCS. In order to determine the optimal proportion, tetracycline hydrochloride, oxytetracycline hydrochloride and chlortetracycline hydrochloride are considered as typical pollutants and their chemical structures are shown in Scheme 1. As seen in Fig. 4 and Fig. S1, the structure of all adsorbents was similar, whereas the adsorption capacity of MWCNT/MIL-53(Fe)-20% was much greater than MWCNT/MIL-53(Fe)-1%, MWCNT/MIL-53(Fe)-5%, MWCNT/MIL-53(Fe)-10%, and MWCNT/MIL-53(Fe)-30%. The excellent adsorption capacity of MWCNT/MIL-53(Fe)-20% could be attribute to the changes of porous structure. As shown in Table 1, the surface area, pore size and total pore volume of MWCNT/MIL-53(Fe)-20% increased sharply after MWCNT modification. Hence, MWCNT/MIL-53(Fe)-20% as the preferred proportion was used in the whole process of research.

3.3. Adsorption kinetics

The effects of time on the TCS adsorption of the MWCNT, MIL-53(Fe) and MWCNT/MIL-53(Fe) composites are shown in Fig. S2. It is quite clear that adsorption performance of MWCNT/MIL-53(Fe) for the TCS is better than MWCNT and MIL-53(Fe). This was because the dispersion of MWCNT/MIL-53(Fe) was better after a small number of MWCNT were introduced, which could make more active sites contact with TCS and increase the adsorption capacity of MWCNT/MIL-53(Fe) for TCS.

Table 1
Parameters of the porous structure for adsorbents.

Sample	$S_{BET}(m^2 \cdot g^{-1})$	$V_t(cm^3 \cdot g^{-1})$	$V_{mic}(cm^3 \cdot g^{-1})$	$V_{mes}(cm^3 \cdot g^{-1})$	$V_{mac}(cm^3 \cdot g^{-1})$	Pore size(nm)
MIL-53(Fe)	52.18	0.115	0.004	0.066	0.045	8.81
MWCNT	136.99	0.400	0.005	0.279	0.116	11.67
MWCNT/MIL-53(Fe)	60.17	0.182	0.004	0.108	0.070	12.09

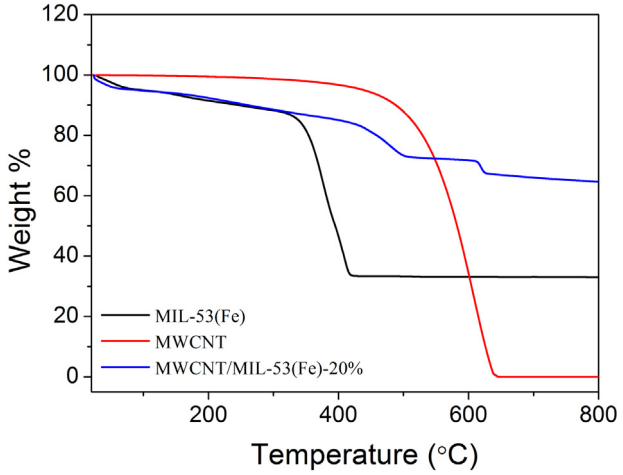

Fig. 3. Thermogravimetric analysis profiles of MIL-53(Fe), MWCNT and MWCNT/MIL-53(Fe)-20%. Flow rate of N_2, 100 mL·min^{-1}; ramping rate, 10 °C min^{-1}.

Adsorption kinetics of all samples is presented in Fig. 6. The adsorption data are fitted to the pseudo-first-order (Eq. (1)) and pseudo-second-order (Eq. (2)) models (H.F. Xiong et al., 2017; W.P. Xiong et al., 2017):

$$q_t = q_e(1- \exp(-k_1 t)) \quad (1)$$

$$q_t = \frac{q_e^2 k_2 t}{1 + q_e k_2 t} \quad (2)$$

where q_e and q_t (mg·g^{-1}) represent the adsorption capacity at equilibrium time and time t (min), and k_1 (min^{-1}), k_2 (g·mg^{-1}·min^{-1}) are the adsorption rate constant of the two kinetic models, respectively.

The model parameters for kinetics have been determined by the average relative error (ARE), and the equation was shown in as follow (Zhou et al., 2017b):

$$ARE = \sum_{i=1}^{n} \left| \frac{Q_{e,\,exp} - Q_{e,cal}}{Q_{e,\,exp}} \right| \quad (3)$$

where "*exp*" and "*cal*" show the experimental and calculated values, respectively.

The kinetic parameters of TCS onto the tested adsorbents are summarized in Table 2. Comparing with the determination coefficients (R^2) and average relative error (ARE) of the pseudo-first-order and pseudo-second-order, it could be suggested that the pseudo-second-order model was better fitted with the experimental data. Furthermore, the adsorption capacity calculated $q_{e,cal}$ from pseudo-second-order equation was more consistent with the experimental $q_{e,exp}$ values. The pseudo-second-order rate model suggested that chemisorptions occurred between TCS and all sorbents maybe involve exchange of electrons or valency forces, which will be discussed in detail on the study of adsorption mechanism.

3.4. Adsorption isotherms

The adsorption isotherm investigations are implemented under room temperature with different initial TCS concentrations. As showed in Fig. S3, the adsorption amount of TCS increases until their equilibrium and remains unchanged. The reason may be that the high initial TCS concentration provides the strength driving force to overcome the mass transfer resistances (H.F. Xiong et al., 2017; W.P. Xiong et al., 2017). The equilibrium adsorption data for the adsorption of TCS by all adsorbents were analyzed by the Langmuir and Freundlich isotherm equations (Eqs. (4) and (5)):

$$q_e = \frac{q_m K_L C_e}{1 + K_L C_e} \quad (4)$$

$$q_e = K_F C_e^{1/n} \quad (5)$$

where q_m (mg·g^{-1}) is the maximum amount of adsorption, q_e (mg·g^{-1}) is the amount of the TCS adsorbed at equilibrium and K_L (L·mg^{-1}) is the Langmuir constant related to the adsorption energy. K_F (L·mg^{-1}) and $1 \cdot n^{-1}$ are Freundlich constants representing for the adsorption capacity and the intensity of adsorption, respectively (Z.B. Wu et al., 2016; H.P. Wu et al., 2016). Moreover, the model parameters for Langmuir and Freundlich isotherms have also been determined by the average relative error (ARE) using the iterative method.

The isotherm parameters of Langmuir and Freundlich isotherms for the TCS adsorption are listed in Table 3. It was obvious that the determination coefficients (R^2) of Langmuir model were much higher than that of Freundlich isotherm model for all adsorbents, and the Langmuir isotherm model showed lower values of average relative errors (ARE), which demonstrated that Langmuir model fitted the experiment data better than Freundlich isotherm model (Fig. 7) and the homogeneous adsorption of TCS occurred on the adsorbents. Compared with MWCNT and MIL-53(Fe), the maximum adsorption capacity ($q_{m,cal}$) calculated from Langmuir model of the MWCNT/MIL-53(Fe) composites were larger than MWCNT and MIL-53(Fe), where TCS predominated. In addition, the adsorption capacities of TCS on MWCNT/MIL-53(Fe) were compared with other adsorbents, and the results were shown in Table S-1. It was easy to see that the adsorption capacity of MWCNT/MIL-53(Fe) was greater than that of other adsorbents.

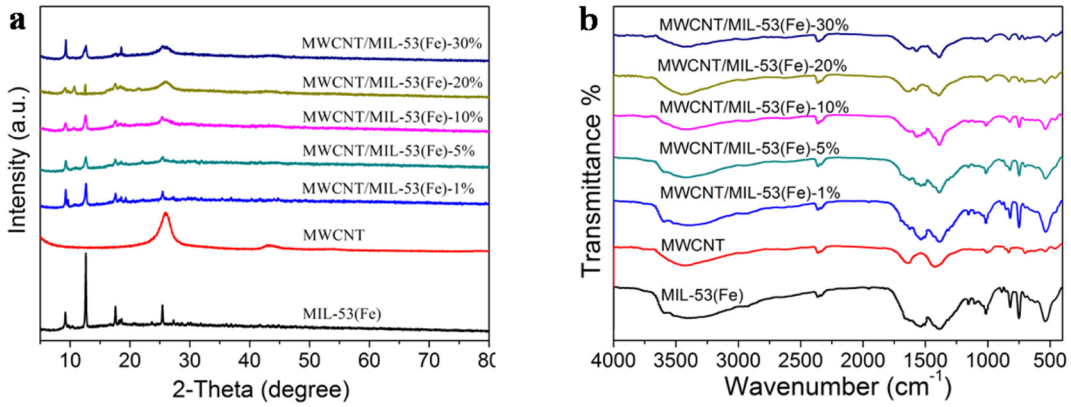

Fig. 4. The XRD spectrum (a), FT-IR absorption spectra (b) of MIL-53(Fe), MWCNT and MWCNT/MIL-53(Fe).

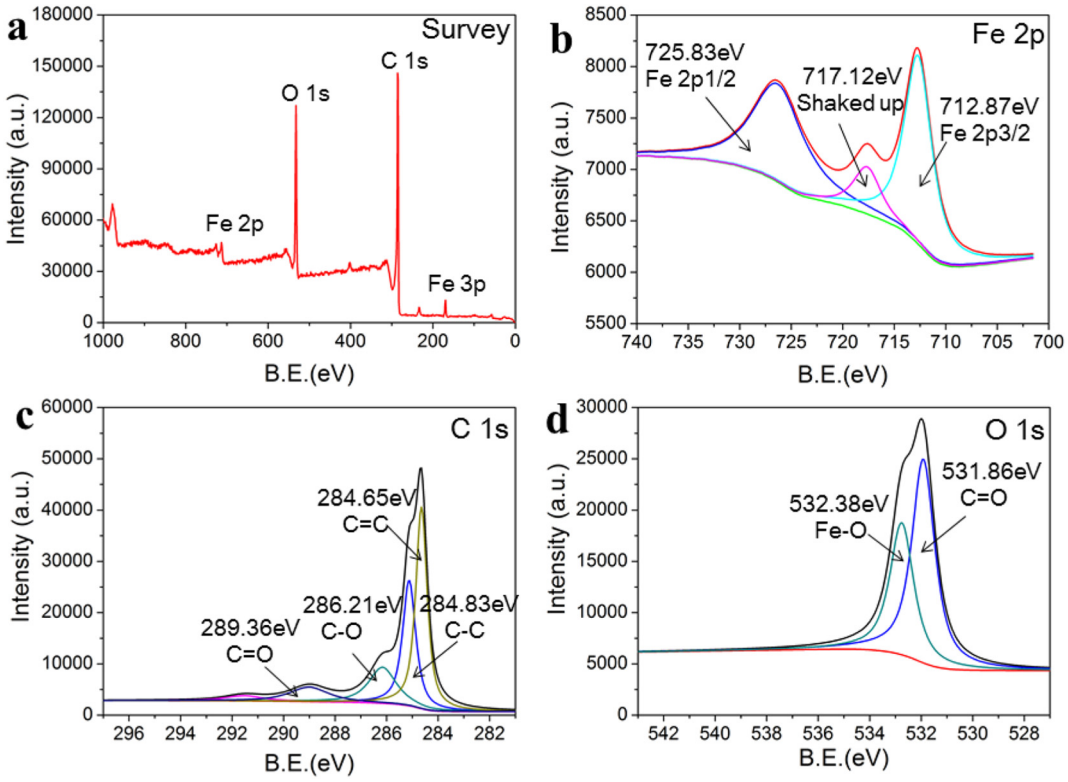

Fig. 5. The XPS spectra of MWCNT/MIL-53(Fe): (a) the full XPS spectra of MWCNT/MIL-53(Fe)-20%, (b) Fe 2p, (c) C 1s and (d) O 1s.

For an in-depth analysis of Langmuir isotherm, a dimensionless constant separation factor (R_L) is used as follows:

$$R_L = \frac{1}{1 + K_L C_0} \tag{6}$$

Where, the value of R_L shows whether or not corresponds to the Langmuir isotherm. K_L ($L \cdot mg^{-1}$) is the Langmuir constant and C_0 ($mg \cdot L^{-1}$) is the original concentration of TCS. From Table 3, the values of R_L for all samples are between 0 and 1. Furthermore, the R_L values of MWCNT/MIL-53(Fe) are smaller than MWCNT and MIL-53(Fe), indicating that the type of Langmuir isotherm is favorable.

3.5. Effects of pH and ionic strength on antibiotic adsorption

The effect of pH ranging from 3.0 to 9.0 on the adsorption capacity of MWCNT/MIL-53(Fe) is shown in Fig. S4. In order to better understand the effect of pH on adsorption, the zeta potential of the adsorbents was showed in Fig. S5, and dissociation constants (pKa) of TCN, OTC and CTC were 3.32, 7.78, 9.58 and 3.22, 7.46, 8.94 and 3.33, 7.55, 9.33, respectively (Qiang and Adams, 2004). As seen in Fig. S5, the isoelectric points of MWCNT/MIL-53(Fe) was approximately 6.75. It was clear that the amounts of adsorbed TCS had a reduction in adsorption at higher pH values, demonstrating the role of electrostatic repulsion between adsorbents and TCS.

The effects of presence of ionic strength on the adsorption of TCS were showed in Fig. S6. It could be obviously found that the amounts of TCN, OTC and CTC adsorbed on MWCNT/MIL-53(Fe) severally decreased with the increase of NaCl concentration because Na^+ may compete with TCS for the same active site of the adsorbents via donor-acceptor interaction.

3.6. Possible mechanisms for tetracycline adsorption

It is important for efficient removal of contaminants to explore the possible mechanism of adsorption. Normally, adsorption mechanisms of MOFs include electrostatic interaction, hydrogen bonding, π-π interactions, pore/size-selective adsorption, etc. In order to study the adsorption mechanism, the pH of TCS solution was varied from 3 to 9, because the pH had a considerable influence on physicochemical property of not only the adsorbate but also the adsorbent (Seo et al., 2017). In Section 3.5, it can be seen that TCN (OTC and CTC) has positive charge at pH < 3.32 (3.22 and 3.33), neutral charge at 3.32 (3.22 and 3.33) < pH < 7.78 (7.46 and 7.55), and negative charge at pH > 7.78 (7.46 and 7.55). On the other hand, MWCNT/MIL-53(Fe) has positive and negative surface charge at pH < 6.75 and pH > 6.75, respectively, based on their zeta potentials. However, the decrease rate of q_e was slower at pH >

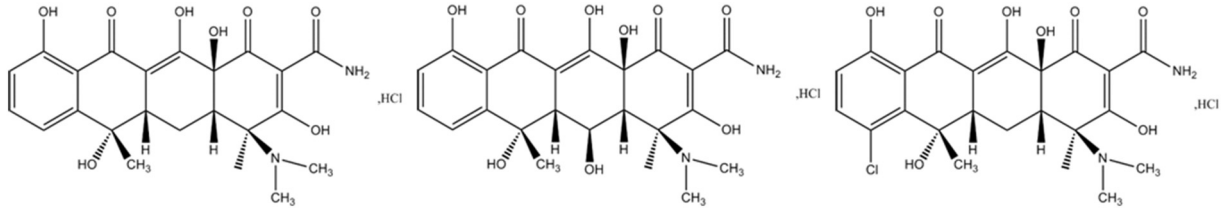

Scheme 1. Chemical structures of Tetracycline Hydrochloride (TCN: 480.9), Oxytetracycline Hydrochloride (OTC: 496.9) and Chlortetracycline Hydrochloride (CTC: 515.3).

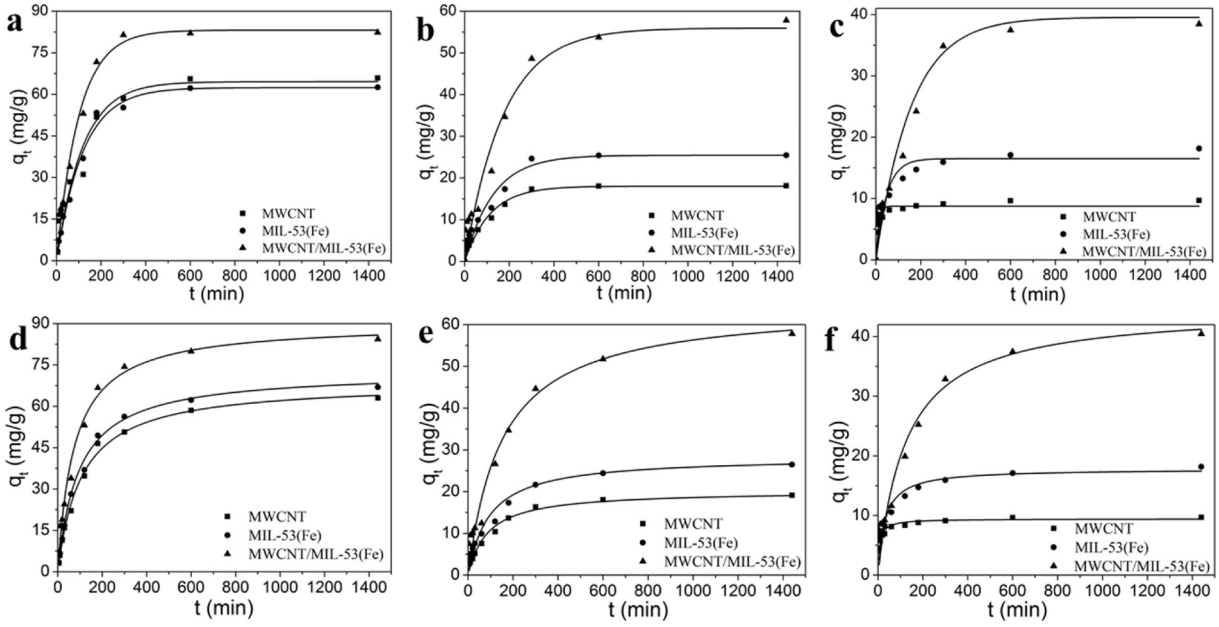

Fig. 6. The pseudo-first order plots for TCN (a), OTC (b) and CTC (c) adsorption; the pseudo-second order plots for TCN (d), OTC (e) and CTC (f) adsorption. Reaction conditions: TCN, OTC and CTC concentration = 20 mg·L^{-1}, respectively; adsorbent loading = 0.2 g·L^{-1}; temperature = 25 °C; initial pH = 7.

7.78 (7.46 and 7.55) than at 3.32 (3.22 and 3.33) < pH < 7.78 (7.46 and 7.55), indicating electrostatic interaction was not main mechanism for adsorption behind the high-efficient adsorption of TCS over MWCNT/MIL-53(Fe).

The q_e of MWCNT/MIL-53(Fe) decreased with pH increasing, which could be the explanation for the influence of unsaturated metal sites. The interaction at high pH may occur between unsaturated metal sites with OH^- in solutions, causing a competitive adsorption of OH^- and contaminants (Tong et al., 2013). However, there still presented a certain adsorption amount of TCS when the pH value increased to 9, which resulted from π–π stacking between the benzene rings of the TCS and the virgin MOFs (Huo and Yan, 2012). Besides, electron cloud density of benzene rings is an essential factor for TCS adsorption. The electron cloud density of benzene rings decreases in the order: TCN > OTC > CTC, similar to the order of their adsorption capacity, indicating that larger electron cloud density of TCS corresponds to the stronger adsorption capacity of adsorbents. Dispersive π-π adsorbate-adsorbent interactions are main mechanism for adsorption.

Pore/size-selective adsorption, determined by the adsorbate molecule magnitude and adsorbent dimensions, is also considered as a

Table 2
Adsorption kinetics parameters of TCN, OTC and CTC onto adsorbents.

Pollutants	Kinetics	Parameters	Adsorbents		
			MWCNT	MIL-53(Fe)	MWCNT/MIL-53(Fe)
TCN	Pseudo-first-order kinetic	$q_{e,exp}$(mg·g^{-1})	65.88	62.53	82.35
		k_1(1/h)	8.6×10^{-3}	8.4×10^{-3}	9.8×10^{-3}
		$q_{e,cal}$(mg·g^{-1})	64.57 ± 3.98	62.42 ± 1.68	83.16 ± 2.72
		ARE	0.398	0.228	0.287
		R^2	0.932	0.989	0.980
	Pseudo-second-order kinetic	k_2(g/(mg·h))	1.4×10^{-4}	1.5×10^{-4}	1.5×10^{-4}
		$q_{e,cal}$(mg·g^{-1})	68.68 ± 1.62	72.70 ± 1.78	89.21 ± 2.81
		ARE	0.155	0.088	0.182
		R^2	0.994	0.997	0.996
OTC	Pseudo-first-order kinetic	$q_{e,exp}$(mg·g^{-1})	18.13	25.45	53.79
		k_1(1/h)	8.8×10^{-3}	7.8×10^{-3}	5.7×10^{-3}
		$q_{e,cal}$(mg·g^{-1})	18.03 ± 0.71	25.46 ± 1.51	55.96 ± 3.76
		ARE	0.145	0.228	0.319
		R^2	0.974	0.943	0.944
	Pseudo-second-order kinetic	k_2(g/(mg·h))	5.7×10^{-4}	3.7×10^{-4}	1.5×10^{-4}
		$q_{e,cal}$(mg·g^{-1})	20.18 ± 0.96	28.31 ± 1.62	60.83 ± 1.98
		ARE	0.087	0.098	0.123
		R^2	0.995	0.994	0.985
CTC	Pseudo-first-order kinetic	$q_{e,exp}$(mg·g^{-1})	10.69	18.16	38.46
		k_1(1/h)	9.8×10^{-2}	2.1×10^{-2}	6.3×10^{-3}
		$q_{e,cal}$(mg·g^{-1})	8.74 ± 0.56	16.50 ± 1.38	39.54 ± 3.03
		ARE	0.358	0.370	0.212
		R^2	0.784	0.778	0.917
	Pseudo-second-order kinetic	k_2(g/(mg·h))	3.7×10^{-3}	1.9×10^{-3}	1.8×10^{-4}
		$q_{e,cal}$(mg·g^{-1})	11.75 ± 0.12	18.53 ± 0.17	43.08 ± 1.78
		ARE	0.115	0.108	0.190
		R^2	0.994	0.996	0.989

Table 3
Isotherm parameters for the adsorption of TCN, OTC and CTC onto adsorbents.

Pollutants	Isotherms	Parameters	Adsorbents		
			MWCNT	MIL-53(Fe)	MWCNT/MIL-53(Fe)
TCN	Langmuir	$q_{m,cal}(mg\cdot g^{-1})$	291.57 ± 14.62	298.00 ± 9.84	364.37 ± 20.21
		$K_L(L\cdot mg^{-1})$	2.8×10^{-2}	3.4×10^{-2}	4.4×10^{-2}
		R_L	0.65	0.59	0.53
		ARE	0.160	0.102	0.201
		R^2	0.989	0.994	0.983
	Freundich	$1\cdot n^{-1}$	0.47 ± 0.04	0.43 ± 0.04	0.40 ± 0.03
		$K_F(L\cdot mg^{-1})$	24.34 ± 4.43	31.24 ± 5.61	47.74 ± 6.25
		ARE	0.385	0.392	0.351
		R^2	0.968	0.964	0.977
OTC	Langmuir	$q_{m,cal}(mg\cdot g^{-1})$	39.34 ± 3.80	226.18 ± 10.72	325.59 ± 18.20
		$K_L(L\cdot mg^{-1})$	3.0×10^{-2}	1.0×10^{-2}	1.1×10^{-2}
		R_L	0.63	0.83	0.82
		ARE	0.250	0.142	0.151
		R^2	0.942	0.996	0.995
	Freundich	$1\cdot n^{-1}$	0.43 ± 0.09	0.62 ± 0.05	0.62 ± 0.05
		$K_F(L\cdot mg^{-1})$	3.85 ± 1.53	6.28 ± 1.55	9.16 ± 2.24
		ARE	0.531	0.361	0.364
		R^2	0.856	0.972	0.972
CTC	Langmuir	$q_{m,cal}(mg\cdot g^{-1})$	54.15 ± 2.80	160.43 ± 11.58	180.68 ± 10.90
		$K_L(L\cdot mg^{-1})$	1.4×10^{-2}	1.3×10^{-2}	4.2×10^{-2}
		R_L	0.78	0.79	0.54
		ARE	0.121	0.138	0.193
		R^2	0.992	0.987	0.973
	Freundich	$1\cdot n^{-1}$	0.52 ± 0.04	0.55 ± 0.06	0.38 ± 0.04
		$K_F(L\cdot mg^{-1})$	2.78 ± 0.55	6.85 ± 1.87	24.82 ± 3.86
		ARE	0.352	0.401	0.387
		R^2	0.974	0.957	0.966

major mechanism of adsorption. As stated in Table 1, MWCNT/MIL-53 (Fe) is primarily composed of micropore and macropore volume, providing a larger surface fraction. It is well known that the size of molecules decreases in the order: CTC > OTC > TCN (Rivera-Utrilla et al., 2013). The small molecular TCN is more likely to enter the pores and be combined with active sites of MWCNT/MIL-53(Fe), thus TCN can be easily removed by adsorption. As mentioned above, the result of the adsorption capacity of adsorbents for TCS is also relevant to the size of TCS molecules.

3.7. Reusability and stability of MWCNT/MIL-53(Fe)

It is important for commercial applications of an adsorbent to evaluate its reusability. In this study, the reusability of MWCNT/MIL-53(Fe) was evaluated after washing the used adsorbents with ethyl alcohol and drying them at 150 °C for reuse. As shown in Fig. S7(a), the performance of reusable adsorbents did not change obviously after reusing four times for TCS.

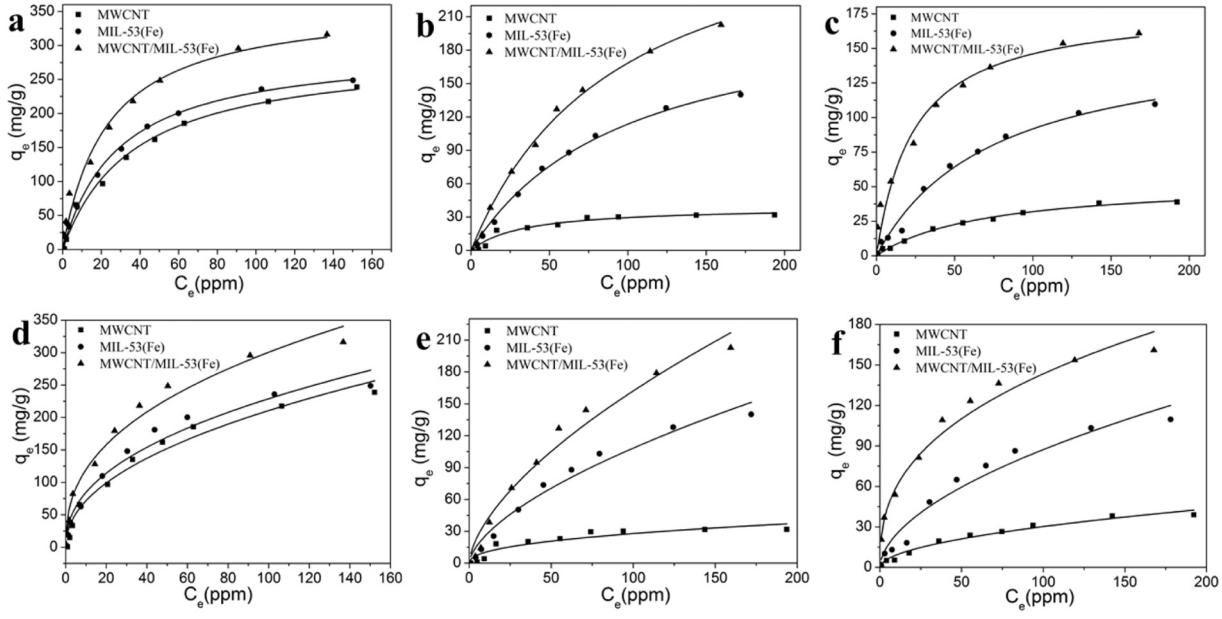

Fig. 7. The Langmuir isotherm model for TCN (a), OTC (b) and CTC (c) adsorption; the Frendich isotherm model for TCN (d), OTC (e) and CTC (f) adsorption. Reaction conditions: adsorbent loading = 0.2 g·L^{-1}; temperature = 25 °C; initial pH = 7.

Previous studies showed that some MOFs had a weak water stability, which limited practical applications in aqueous solutions. In this study, MOF materials were combined with MWCNT to enhance the water stability of MOF materials. As shown in Fig. S7(b), the FT-IR spectra of reusable MWCNT/MIL-53(Fe) showed it was very similar to that of the fresh MWCNT/MIL-53(Fe), indicating structural stability of MWCNT/MIL-53 (Fe). Besides, compared to the fresh MWCNT/MIL-53(Fe), the SEM of reusable MWCNT/MIL-53(Fe) remained unchanged in Fig. S7(c). In order to further study the stability of adsorbent, MWCNT/MIL-53(Fe) was entirely submerged in aqueous solutions and the concentration of iron ions was detected consecutively in 30 days. As seen in Fig. S7(d), there was a sharp increase in iron ions concentration in aqueous solutions from day 0 to day 3. After that, the concentration of iron ions remained the same. However, the concentration of iron ions in MIL-53(Fe) containing aqueous solutions was twice than that in aqueous solutions which contained MWCNT/MIL-53(Fe), demonstrating that the water stability of MIL-53(Fe) modified by MWCNT had been enhanced.

4. Conclusions

In this study, MWCNT/MIL-53(Fe) has been successfully synthesized and used for adsorption in TCN, OTC and CTC from aqueous solutions. The specific surface area, pore volume and pore diameter of MWCNT/MIL-53(Fe) were 1.2, 1.6 and 1.4 times than that of MIL-53(Fe) due to the modification of MWCNT. And its thermal stability was increased, but the crystalline structures were not changed. It was found that the adsorption kinetics and isotherms for TCS with MWCNT/MIL-53(Fe) were better fitted with pseudo-second-order model and Langmuir model. The adsorption capacity for TCS adsorption onto MWCNT/MIL-53(Fe) was much larger than that of MWCNT and MIL-53(Fe). In addition to π-π adsorbate-adsorbent interactions, the adsorption mechanisms were also ascribed to pore/size-selective adsorption and influence of framework metal ions in adsorption. After washed by a cushy method, the reusable adsorbent maintained original physicochemical properties. The FT-IR spectra and SEM of reusable MWCNT/MIL-53(Fe) as well as the concentration of iron ions in aqueous solutions containing MWCNT/MIL-53(Fe) revealed its water stability. Therefore, these advantages indicate that MWCNT/MIL-53(Fe) is a promising adsorbent for removal of TCS in aqueous solutions.

Acknowledgements

The study was financially supported by the National Natural Science Foundation of China (51521006, 51378190, 51578223 and 51709103), the Program for Changjiang Scholars and Innovative Research Team in University (IRT-13R17), the Fundamental Research Funds for the Central Universities (531107051080) and the Key Research and Development Program of Hunan Province (2017SK2242).

Appendix A. Supplementary data

Supplementary data to this article can be found online at https://doi.org/10.1016/j.scitotenv.2018.01.249.

References

Ahmed, M.J., 2017. Adsorption of quinolone, tetracycline, and penicillin antibiotics from aqueous solution using activated carbons. Environ. Toxicol. Pharmacol. 50, 1–10.
Ai, L.H., Li, L.L., Zhang, C.H., Fu, J., Jiang, J., 2013. MIL-53(Fe): a metal-organic framework with intrinsic peroxidase-like catalytic activity for colorimetric biosensing. Chem. Eur. J. 19, 15105–15108.
Araya, T., Jia, M., Yang, J., Zhao, P., Cai, K., Ma, W.H., Huang, Y.P., 2017. Resin modified MIL-53 (Fe) MOF for improvement of photocatalytic performance. Appl. Catal. B Environ. 203, 768–777.
Azhar, M.R., Abid, H.R., Sun, H., Periasamy, V., Tadé, M.O., Wang, S.B., 2016. Excellent performance of copper based metal organic framework in adsorptive removal of toxic sulfonamide antibiotics from wastewater. J. Colloid Interface Sci. 478, 344–352.
Azhar, M.R., Abid, H.R., Periasamy, V., Sun, H., Tade, M.O., Wang, S.B., 2017. Adsorptive removal of antibiotic sulfonamide by UiO-66 and ZIF-67 for wastewater treatment. J. Colloid Interface Sci. 500, 88–95.
Azhar, M.R., Vijay, P., Tadé, M.O., Sun, H.Q., Wang, S.B., 2018. Submicron sized water-stable metal organic framework (bio-MOF-11) for catalytic degradation of pharmaceuticals and personal care products. Chemosphere 196, 105–114.
Barea, E., Montoro, C., Navarro, J.A.R., 2014. Toxic gas removal-metal-organic frameworks for the capture and degradation of toxic gases and vapours. Chem. Soc. Rev. 43, 5419–5430.
Cadiaul, A., Belmabkhout, Y., Adil, K., Bhatt, P.M., Pillai, R.S., Shkurenko, A., Corcos, C.M., Maurin, G., Eddaoudi, M., 2017. Hydrolytically stable fluorinated metal-organic frameworks for energy-efficient dehydration. Science 356, 731–735.
Chen, M., Xu, P., Zeng, G.M., Yang, C.P., Huang, D.L., Zhang, J.C., 2015. Bioremediation of soils contaminated with polycyclic aromatic hydrocarbons, petroleum, pesticides, chlorophenols and heavy metals by composting: applications, microbes and future research needs. Biotechnol. Adv. 33, 745–755.
Cheng, Y., He, H.J., Yang, C.P., Zeng, G.M., Li, X., Chen, H., Yu, G.L., 2016. Challenges and solutions for biofiltration of hydrophobic volatile organic compounds. Biotechnol. Adv. 34, 1091–1102.
Cheng, M., Zeng, G.M., Huang, D.L., Lai, C., Xu, P., Zhang, C., Liu, Y., 2016a. Hydroxyl radicals based advanced oxidation processes (AOPs) for remediation of soils contaminated with organic compounds: a review. Chem. Eng. J. 284, 582–598.
Cheng, M., Zeng, G.M., Huang, D., Lai, C., Xu, P., Zhang, C., Liu, Y., Wan, J., Gong, X., Zhu, Y., 2016b. Degradation of atrazine by a novel Fenton-like process and assessment the influence on the treated soil. J. Hazard. Mater. 312, 184–191.
Deng, J.H., Zhang, X.R., Zeng, G.M., Gong, J.L., Niu, Q.Y., Liang, J., 2013. Simultaneous removal of cd(II) and ionic dyes from aqueous solution using magnetic graphene oxide nanocomposite as an adsorbent. Chem. Eng. J. 226, 189–200.
Du, J.J., Yuan, Y.P., Sun, J.X., Peng, F.M., Jiang, X., Qiu, L.G., Xie, A.J., Shen, Y.H., Zhu, J.F., 2011. New photocatalysts based on MIL-53 metal–organic frameworks for the decolorization of methylene blue dye. J. Hazard. Mater. 190, 945–951.
Eguilaz, M., Villalonga, R., Yanez-Sedeno, P., Pingarron, J.M., 2011. Designing electrochemical interfaces with functionalized magnetic nanoparticles and wrapped carbon nanotubes as platforms for the construction of high-performance bienzyme biosensors. Anal. Chem. 83, 7807–7814.
Evgenidou, E.N., Konstantinou, I.K., Lambropoulou, D.A., 2015. Occurrence and removal of transformation products of PPCPs and illicit drugs in wastewaters: a review. Sci. Total Environ. 505, 905–926.
Furukawa, H., Cordova, K.E., O'Keeffe, M., Yaghi, O.M., 2013. The chemistry and applications of metal-organic frameworks. Science 341, 1230444.
Gao, Y.W., Li, S.M., Li, Y.X., Yao, L.Y., Zhang, H., 2017. Accelerated photocatalytic degradation of organic pollutant over metal-organic framework MIL-53 (Fe) under visible LED light mediated by persulfate. Appl. Catal. B Environ. 202, 165–174.
Gong, J.L., Wang, B., Zeng, G.M., Yang, C.P., Niu, C.G., Niu, Q.Y., Zhou, W.J., Liang, Y., 2009. Removal of cationic dyes from aqueous solution using magnetic multi-wall carbon nanotube nanocomposite as adsorbent. J. Hazard. Mater. 164, 1517–1522.
Guo, Y.G., Huang, W.L., Chen, B., Zhao, Y., Liu, D.F., Sun, Y., Gong, B., 2017. Removal of tetracycline from aqueous solution by MCM-41-zeolite A loaded nano zero valent iron: synthesis, characteristic, adsorption performance and mechanism. J. Hazard. Mater. 339, 22–32.
Hasan, Z., Khan, N.A., Jhung, S.H., 2016. Adsorptive removal of diclofenac sodium from water with Zr-based metal-organic frameworks. Chem. Eng. J. 284, 1406–1413.
Hu, T.D., Lv, H.T., Shan, S.Y., Jia, Q.M., Su, H.Y., Tian, N., He, S.C., 2016. Porous structured MIL-101 synthesized with different mineralizers for adsorptive removal of oxytetracycline from aqueous solution. RSC Adv. 6, 73741–73747.
Hu, L., Wan, J., Zeng, G.M., Chen, A.W., Chen, G.Q., Huang, Z.Z., He, K., Cheng, M., Zhou, C.Y., Xiong, W.P., Lai, C., Xu, P., 2017. Comprehensive evaluation of the cytotoxicity of CdSe/ZnS quantum dots in Phanerochaete chrysosporium by cellular uptake and oxidative stress. Environ. Sci. Nano https://doi.org/10.1039/C7EN00517B.
Huang, X., Tan, C.L., Yin, Z.Y., Zhang, H., 2014. 25th anniversary article: hybrid nanostructures based on two-dimensional nanomaterials. Adv. Mater. 26, 2185–2204.
Huo, S.H., Yan, X.P., 2012. Metal-organic framework MIL-100(Fe) for the adsorption of malachite green from aqueous solution. J. Mater. Chem. 22, 7449–7455.
Hwang, Y.K., Hong, D.Y., Chang, J.S., Jhung, S.H., Seo, Y.K., Kim, J.H., Vimont, A., Daturi, M., Serre, C., Férey, G., 2008. Amine grafing on coordinatively unsaturated metal centers of MOFs: consequences for catalysis and metal encapsulation. Angew. Chem. Int. Ed. 47, 4144–4148.
Khan, N.A., Hasan, Z., Jhung, S.H., 2013. Adsorptive removal of hazardous materials using metal-organic frameworks (MOFs): a review. J. Hazard. Mater. 244, 444–456.
Liang, R.W., Jing, F.F., Shen, L.J., Qin, N., Wu, L., 2015. MIL-53(Fe) as a highly efficient bifunctional photocatalyst for the simultaneous reduction of Cr (VI) and oxidation of dyes. J. Hazard. Mater. 287, 364–372.
Liang, J., Yang, Z.X., Tang, L., Zeng, G.M., Yu, M., Li, X.D., Wu, H.P., Qian, Y.Y., Li, X.M., Luo, Y., 2017. Changes in heavy metal mobility and availability from contaminated wetland soil remediated with combined biochar-compost. Chemosphere 181, 281–288.
Liu, Z.M., Zhu, M.F., Zhao, L., Deng, C., Ma, J., Wang, Z., Liu, H.B., Wang, H., 2017. Aqueous tetracycline degradation by coal-based carbon electrocatalytic filtration membrane: effect of nano antimony-doped tin dioxide coating. Chem. Eng. J. 314, 59–68.
Liu, X.C., Yang, D.X., Zhou, Y.Y., Zhang, J.C., Luo, L., Meng, S.J., Chen, S., Tan, M.J., Li, Z.C., Tang, L., 2017a. Electrocatalytic properties of N-doped graphite felt in electro-Fenton process and degradation mechanism of levofloxacin. Chemosphere 182, 306–315.
Liu, X.C., Zhou, Y.Y., Zhang, J.C., Tang, L., Luo, L., Zeng, G.M., 2017b. Iron containing metal-organic frameworks: structure, synthesis, and applications in environmental remediation. ACS Appl. Mater. Interfaces 9, 20255–20275.

Long, F., Gong, J.L., Zeng, G.M., Chen, L., Wang, X.Y., Deng, J.H., Niu, Q.Y., Zhang, H.Y., Zhang, X.R., 2011. Removal of phosphate from aqueous solution by magnetic Fe-Zr binary oxide. Chem. Eng. J. 171, 448–455.
Naeimi, S., Faghihian, H., 2017. Application of novel metal organic framework, MIL-53(Fe) and its magnetic hybrid: for removal of pharmaceutical pollutant, doxycycline from aqueous solutions. Environ. Toxicol. Pharmacol. 53, 121–132.
Qiang, Z., Adams, C., 2004. Potentiometric determination of acid dissociation constants (pKa) for human and veterinary antibiotics. Water Res. 38, 2874–2890.
Ramirez, A.J., Brain, R.A., Usenko, S., Mottaleb, M.A., O'Donnell, J.G., Stahl, L.L., Wathen, J.B., Snyder, B.D., Pitt, J.L., Perez-Hurtado, P., Dobbins, L.L., Brooks, B.W., Chambliss, C.K., 2009. Occurrence of pharmaceuticals and personal care products in fish: results of a national pilot study in the United States. Environ. Toxicol. Chem. 28, 2587–2597.
Reed, D.A., Xiao, D.J., Gonzalez, M.I., Darago, L.E., Herm, Z.R., Grandjean, F., Long, J.R., 2016. Reversible CO scavenging via adsorbate-dependent spin state transitions in an iron (II)–triazolate metal–organic framework. J. Am. Chem. Soc. 138, 5594–5602.
Rehman, A., Tirmizi, S.A., Badshah, A., Ammad, H.M., Jawad, M., Abbas, S.M., Rana, U.A., Khan, S.U., 2017. Synthesis of highly stable MOF-5@ MWCNTs nanocomposite with improved hydrophobic properties. Arab. J. Chem. https://doi.org/10.1016/j.arabjc.01.012.
Rivera-Utrilla, J., Gómez-Pacheco, C.V., Sánchez-Polo, M., López-Peñalver, J.J., Ocampo-Pérez, R., 2013. Tetracycline removal from water by adsorption/bioadsorption on activated carbons and sludge-derived adsorbents. J. Environ. Manag. 131, 16–24.
Seo, P.W., Khan, N.A., Jhung, S.H., 2017. Removal of nitroimidazole antibiotics from water by adsorption over metal–organic frameworks modified with urea or melamine. Chem. Eng. J. 315, 92–100.
Song, H.Q., Zhu, Q., Zheng, X.J., Chen, X.G., 2015. One-step synthesis of three-dimensional graphene/multiwalled carbon nanotubes/Pd composite hydrogels: an efficient recyclable catalyst for Suzuki coupling reactions. J. Mater. Chem. A 3, 10368–10377.
Tan, X.F., Liu, Y.G., Zeng, G.M., Wang, X., Hu, X.J., Gu, Y.L., Yang, Z.Z., 2015. Application of biochar for the removal of pollutants from aqueous solutions. Chemosphere 125, 70–85.
Tang, W.W., Zeng, G.M., Gong, J.L., Liang, J., Xu, P., Zhang, C., Huang, B.B., 2014. Removal of heavy metals from aqueous solutions using nanomaterials affected by humic/fulvic acid: a review. Sci. Total Environ. 468-469, 1014–1027.
Tanoue, R., Nomiyama, K., Nakamura, H., Kim, J.W., Isobe, T., Shinohara, R., Tanabe, S., 2015. Uptake and tissue distribution of pharmaceuticals and personal care products in wild fish from treated wastewater-impacted streams. Environ. Sci. Technol. 49, 11649–11658.
Thi, V.H.T., Lee, B.K., 2017. Great improvement on tetracycline removal using ZnO rod-activated carbon fiber composite prepared with a facile microwave method. J. Hazard. Mater. 324, 329–339.
Tong, M.M., Liu, D.H., Yang, Q.Y., Devautour-Vinot, S., Maurin, G., Zhong, C., 2013. Influence of framework metal ions on the dye capture behavior of MIL-100 (Fe, Cr) MOF type solids. J. Mater. Chem. A 1, 8534–8537.
Voorde, B.V., Bueken, B., Denayer, J., Vos, D.D., 2014. Adsorptive separation on metal–organic frameworks in the liquid phase. Chem. Soc. Rev. 43, 5766–5788.
Wang, H., Yuan, X.Z., Wu, Y., Zeng, G.M., Dong, H.R., Chen, X.H., Leng, L.J., Wu, Z.B., Peng, L.J., 2016. In situ synthesis of In2S3@MIL-125 (Ti) core–shell microparticle for the removal of tetracycline from wastewater by integrated adsorption and visible-light-driven photocatalysis. Appl. Catal. B Environ. 186, 19–29.
Wang, C.H., Liu, X.L., Demir, N.K., Chen, J.P., Li, K., 2016. Applications of water stable metal–organic frameworks. Chem. Soc. Rev. 45, 5107–5134.
Wu, T.J., Shen, L.J., Luebbers, M., Hu, C.H., Chen, Q.M., Ni, Z., Masel, R.I., 2010. Enhancing the stability of metal-organic frameworks in humid air by incorporating water repellent functional groups. Chem. Commun. 46, 6120–6122.
Wu, X., Conkle, J.L., Ernst, F., Gan, J., 2014. Treated wastewater irrigation: uptake of pharmaceutical and personal care products by common vegetables under field conditions. Environ. Sci. Technol. 48, 11286–11293.
Wu, Z.B., Yuan, X.Z., Zhong, H., Wang, H., Zeng, G.M., Chen, X.H., Wang, H., Zhang, L., Shao, J.G., 2016. Enhanced adsorptive removal of p-nitrophenol from water by aluminum metal–organic framework/reduced graphene oxide composite. Sci. Rep. https://doi.org/10.1038/srep25638.
Wu, H.P., Lai, C., Zeng, G.M., Liang, J., Chen, J., Xu, J.J., Dai, J., Li, X.D., Liu, J.F., Chen, M., Lu, L.H., Hu, L., Wan, J., 2016. The interaction of composting and biochar and its implication for soil amendment and pollution remediation-a review. Crit. Rev. Biotechnol. 6, 1–11.
Xiong, H.F., Zou, D.L., Zhou, D.D., Dong, S.S., Wang, J.W., Rittmann, B.E., 2017. Enhancing degradation and mineralization of tetracycline using intimately coupled photocatalysis and biodegradation (ICPB). Chem. Eng. J. 316, 7–14.
Xiong, W.P., Tong, J., Yang, Z.H., Zeng, G.M., Zhou, Y.Y., Wang, D.B., Song, P.P., Xu, R., Zhang, C., Cheng, M., 2017. Adsorption of phosphate from aqueous solution using iron-zirconium modified activated carbon nanofiber: performance and mechanism. J. Colloid Interface Sci. 493, 17–23.
Xu, P., Zeng, G.M., Huang, D.L., Feng, C.L., Hu, S., Zhao, M.H., Lai, C., Wei, Z., Huang, C., Xie, G.X., Liu, Z.F., 2012a. Use of iron oxide nanomaterials in wastewater treatment: a review. Sci. Total Environ. 424, 1–10.
Xu, P., Zeng, G.M., Huang, D.L., Lai, C., Zhao, M.H., Wei, Z., Li, N.J., Huang, C., Xie, G.X., 2012b. Adsorption of Pb(II) by iron oxide nanoparticles immobilized *Phanerochaete chrysosporium*: equilibrium, kinetic, thermodynamic and mechanisms analysis. Chem. Eng. J. 203, 423–431.
Yang, S.J., Choi, J.Y., Chae, H.K., Cho, J.H., Nahm, K.S., Park, C.R., 2009. Preparation and enhanced hydrostability and hydrogen storage capacity of CNT@ MOF-5 hybrid composite. Chem. Mater. 21, 1893–1897.
Yang, C.P., Chen, H., Zeng, G.M., Yu, G.L., Luo, S.L., 2010. Biomass accumulation and control strategies in gas biofilters. Biotechnol. Adv. 28, 531–540.
Yang, Z.W., Xu, X.Q., Liang, X.X., Cheng, L., Wei, Y.L., He, P.Q., Lv, B.L., Ma, H.C., Lei, Z.Q., 2016. MIL-53(Fe)-graphene nanocomposites: efficient visible-light photocatalysts for the selective oxidation of alcohols. Appl. Catal. B Environ. 198, 112–123.
Ye, J., Du, Y.P., Wang, L.M., Qian, J.R., Chen, J.J., Wu, Q.W., Hu, X.J., 2017. Toxin release of cyanobacterium *Microcystis aeruginosa* after exposure to typical tetracycline antibiotic contaminants. Toxins 9, 53.
Yu, B.W., Bai, Y.T., Ming, Z., Yang, H., Chen, L.Y., Hu, X.J., Feng, S.C., Yang, S.T., 2017. Adsorption behaviors of tetracycline on magnetic graphene oxide sponge. Mater. Chem. Phys. 198, 283–290.
Zeng, G.M., Wan, J., Huang, D.L., Hu, L., Huang, C., Cheng, M., Xue, W.J., Gong, X.M., Wang, R.Z., Jiang, D.L., 2017. Precipitation, adsorption and rhizosphere effect: the mechanisms for phosphate-induced Pb immobilization in soils—a review. J. Hazard. Mater. 339, 354–367.
Zhang, Y., Zeng, G.M., Tang, L., Chen, J., Zhu, Y., He, X.X., He, Y., 2015. Electrochemical sensor based on electrodeposited graphene-Au modified electrode and nano Au carrier amplified signal strategy for attomolar mercury detection. Anal. Chem. 87, 989–996.
Zhang, C., Lai, C., Zeng, G.M., Huang, D.L., Tang, L., Yang, C.P., Zhou, Y.Y., Qin, L., Cheng, M., 2016a. Nanoporous Au-based chronocoulometric aptasensor for amplified detection of Pb2+ using DNAzyme modified with Au nanoparticles. Biosens. Bioelectron. 81, 61–67.
Zhang, C., Lai, C., Zeng, G.M., Huang, D.L., Yang, C.P., Wang, Y., Zhou, Y.Y., Chen, M., 2016b. Efficacy of carbonaceous nanocomposites for sorbing ionizable antibiotic sulfamethazine from aqueous solution. Water Res. 95, 103–112.
Zhou, Y.Y., Liu, X.C., Tang, L., Zhang, F.F., Zeng, G.M., Peng, X.Q., Luo, L., Deng, Y.C., Pang, Y., Zhang, J.C., 2017a. Insight into highly efficient co-removal of p-nitrophenol and lead by nitrogen-functionalized magnetic ordered mesoporous carbon: performance and modeling. J. Hazard. Mater. 333, 80–87.
Zhou, Y.Y., Liu, X.C., Xiang, Y.J., Wang, P., Zhang, J.C., Zhang, F.F., Wei, J.H., Luo, L., Lei, M., Tang, L., 2017b. Modification of biochar derived from sawdust and its application in removal of tetracycline and copper from aqueous solution: adsorption mechanism and modelling. Bioresour. Technol. 245, 266–273.
Zhou, C.Y., Lai, C., Huang, D.L., Zeng, G.M., Zhang, C., Cheng, M., Hu, L., Wan, J., Xiong, W.P., Wen, M., Wen, X.F., Qin, L., 2018. Highly porous carbon nitride by supramolecular preassembly of monomers for photocatalytic removal of sulfamethazine under visible light driven. Appl. Catal. B Environ. 220, 202–210.